Solution of an Elliptic Inverse Convection Problem Using a Whole Domain Regularization Technique

A. Moutsoglou*
South Dakota State University, Brookings, South Dakota 57007

The inverse convection problem for developing laminar forced flow in a channel is investigated. The straight inversion process is found to be susceptible to inherent random errors introduced either by the numerical computations and/or experimental errors. In order to overcome the ill-posed behavior associated with inverse problems, a whole domain regularization scheme tailored for elliptic differential equations is employed in solving the governing energy equation. The methodology is found to be effective in curbing the ill-posed symptoms inherent in inverse problems. When a simple smoothing procedure is tested in conjunction with a straight inversion scheme, it fails to alleviate such symptoms and exhibits highly unstable results.

Nomenclature

A = matrix of coefficients, Eq. (11)
C = dimensionless standard deviation of the bottom wall temperature, Eq. (20)
D = matrix of constants, Eq. (14)
e = Gaussian random error
H = channel width, m
k = thermal conductivity, W/m · K
L = length of channel, m
N = number of axial grid points excluding the channel inlet
P = dimensionless pressure
p = pressure, Pa
Pr = Prandtl number
Q = matrix of top wall heat flux corrections, Eq. (13)
q_T = dimensionless top wall local heat flux $q_{|y=0}/q_{\text{ref}}$
Re = Reynolds number $2\bar{u}H/\nu$
S_j = $\partial\Theta/\partial q_{T,j}$, sensitivity function
s = augmented sum, Eq. (6)
T = temperature, K
U,V = dimensionless axial and transverse velocity components
u,v = axial and transverse velocity components, m/s
$\bar{u}$ = average velocity, m/s
W_0 = coefficient of zeroth order regularization term
W_1 = coefficient of first order regularization term
X,Y = dimensionless axial and transverse coordinates
X_N = dimensionless channel length
x,y = axial and transverse coordinates, m
$Z_{i,j}$ = heat flux sensitivity coefficient of the bottom wall, Eq. (12) or (18)
α = regularization parameter
Δq_T = top wall heat flux correction
ΔX = dimensionless axial stepsize
δ_{ij} = Kronecker delta
ϵ = additive error, Eq. (20)
Θ = dimensionless temperature
ν = kinematic viscosity, m^2/s
ρ = density, kq/m^3
σ = root mean square error of the dimensionless estimated top wall heat flux, Eq. (5)

Introduction

INVERSE convection problems arise in instances when a surface in contact with a moving fluid is inaccessible to instrumentation and no information with regard to the surface thermal boundary conditions is available. The inverse convection problem is defined as the estimation of the heat flux and/or temperature distribution on a surface (boundary) from measured temperature and heat flux distributions along a different surface (boundary) which are in thermal communication via a moving fluid. The ill-posed nature of inverse problems in convective heat transfer environments was recently investigated for free convection flow in a channel.[1] The study revealed that inverse convection problems exhibit trends characteristic of inverse conduction problems. That is, inverse problems fail to satisfy the stability condition that ensures that small changes in data will result in small changes in the solution. Thus, arbitrarily small fluctuations of surface heat flux and/or temperature data arising from inaccuracies in experimental measurements or inherent computational errors, as evidenced by the present study, may result in highly oscillatory and unstable estimations of the surface temperature and heat fluxes. In Ref. 1, the governing conservation equations for free convection flow in a channel were parabolized, and the ill-symptoms of the inversion procedure due to superposed random fluctuations on the direct input data were alleviated by a sequential function specification scheme devised by Beck[2] specifically for the inversion of the parabolic heat diffusion equation.

In this study, a whole domain regularization technique developed by Tikhonov and Arsenin[3] and tailored for elliptic differential equations is adapted for forced convection flow in a channel. The performance of the inverse methodology is assessed for elliptic convective flows and compared to that of a straight inversion scheme with and without a simple smoothing procedure.

Direct Convection Problem

Analysis

In order to provide input data for the inverse problem as well as a criterion for evaluating the performance of the inverse methodology, the direct heat transfer problem is analyzed first.

The study is concerned with forced flow of air in a horizontal channel as shown in Fig. 1. The top surface of the channel is being heated while the bottom surface is insulated. The direct heat transfer problem is defined as one for which thermal boundary conditions are prescribed at both channel walls.

The steady two-dimensional laminar flow equations were nondimensionalized via the following parameters:

$$X = \frac{2x}{HRe}, \qquad Y = \frac{y}{H}, \qquad U = \frac{u}{\bar{u}}, \qquad V = \frac{vRe}{\bar{u}2}$$

$$\Theta = k\frac{T - T_0}{q_{\text{ref}}H}, \qquad P = \frac{p - p_0}{\rho\bar{u}^2} \tag{1}$$

where H is the channel width, $\bar{u}$ is the average velocity, T_0 and p_0 are the uniform temperature and pressure at the inlet of the channel, q_{ref} is some reference heat flux, and Re is the Reynolds number based on the hydraulic diameter, $Re = 2\bar{u}H/\nu$.

Received June 9, 1988; revision received Feb. 28, 1989.

*Associate Professor, Department of Mechanical Engineering.

The governing dimensionless system of equations can then be expressed as

$$\frac{\partial U}{\partial X}+\frac{\partial V}{\partial Y}=0 \tag{2a}$$

$$U\frac{\partial U}{\partial X}+V\frac{\partial U}{\partial Y}=-\frac{\partial P}{\partial X}+\frac{4}{Re^2}\frac{\partial^2 U}{\partial X^2}+\frac{\partial^2 U}{\partial Y^2} \tag{2b}$$

$$U\frac{\partial V}{\partial X}+V\frac{\partial V}{\partial Y}=-\frac{Re^2}{4}\frac{\partial P}{\partial Y}+\frac{4}{Re^2}\frac{\partial^2 V}{\partial X^2}+\frac{\partial^2 V}{\partial Y^2} \tag{2c}$$

$$U\frac{\partial \Theta}{\partial X}+V\frac{\partial \Theta}{\partial Y}=\frac{4}{PrRe^2}\frac{\partial^2 \Theta}{\partial X^2}+\frac{1}{Pr}\frac{\partial^2 \Theta}{\partial Y^2} \tag{2d}$$

where the buoyancy force in the Y-momentum equation has been neglected, and Pr is the Prandtl number of the fluid.

In specifying the relevant boundary conditions, uniform velocity and temperature profiles were assigned at the inlet of the channel. The boundary conditions can thus be written as

$$U=1,\quad V=0,\quad P=0,\quad \Theta=0 \text{ at } X=0 \tag{3a}$$

$$U=0,\quad V=0 \text{ at } Y=0 \quad \text{and} \quad Y=1 \tag{3b}$$

$$\frac{\partial \Theta}{\partial Y}=-q_T(X) \text{ at } Y=0, \qquad \frac{\partial \Theta}{\partial Y}=0 \text{ at } Y=1 \tag{3c}$$

where q_T is the prescribed heat flux at the top surface of the channel, nondimensionalized with respect to the reference heat flux q_{ref}. As no information is available with regard to the outflow boundary, a local one way behavior for the velocity and temperature fields is assumed at the exit of the channel. As a result, the axial diffusion of viscous forces in the X- and Y-momentum equations and the axial diffusion of heat in the energy equation are set equal to zero *only* at the channel exit, eliminating the need for any outflow boundary condition. An assumption such as this is only justified if the corresponding diffusion coefficients of these terms are sufficiently small, a condition that requires high Reynolds and Peclet numbers. However, in view of the lack of any other outflow information, these conditions were assigned in this problem, and the absence of any flow recirculation justified their use.

Computational Procedure and Results

The elliptic governing conservation equations for momentum and energy, Eqs. (2) and (3), were solved by the Simpler algorithm of Patankar.[4] In the finite difference procedure, the power law scheme was employed for treating the convection-diffusion terms. The iterative procedure utilized the tridiagonal matrix algorithm of Thomas in solving the resultant algebraic equations.

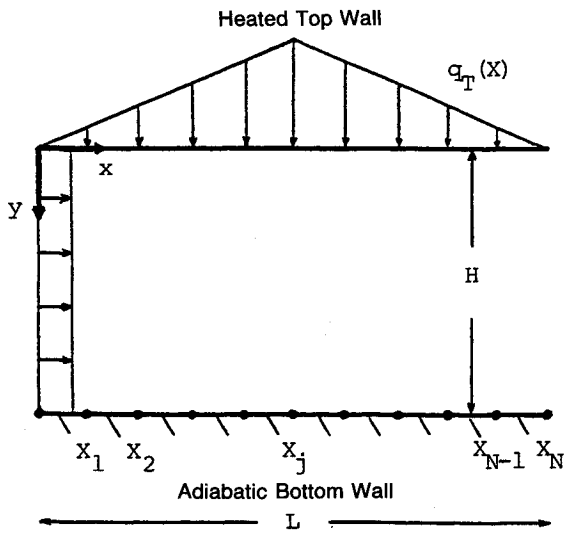

Fig. 1 Flow schematic and coordinate system.

The direct heat transfer problem described by Eqs. (2) and (3) was solved for a prescribed dimensionless triangular heat flux $q_T(X)$, Eq. (3c), at the top surface of the channel.

$$q_T(X)=\begin{cases}\dfrac{20X}{X_N} & \text{for } X\le X_N/2\\[2ex] 20-\dfrac{20X}{X_N} & \text{for } X\ge X_N/2\end{cases} \tag{4}$$

The dimensionless channel length was fixed at $X_N=0.1$, and the Reynolds number and Prandtl number were assigned, respectively, the values of $Re=50$ and $Pr=0.7$. In generating the finite difference mesh, 43 grid points were deployed in the transverse direction. In the streamwise direction, the grid points were placed at equal distance apart $\Delta X=X_N/N$, where X_N is the dimensionless length of the channel, and $N+1$ is the total number of axial grid points as indicated in Fig. 1. The dimensionless temperature variation of the bottom insulated wall $\Theta_{Bd}(X)$, obtained from the direct heat transfer problem employing 21 axial grid points ($N=20$, $\Delta X=0.005$) is depicted in Fig. 2 with the symbol + .

The discrete data $\Theta_{Bd}(X_i)$ at the $N=20$ locations away from the inlet simulate a priori the errorless readings that perfect temperature sensors with zero instrument error, located at these twenty X_i ($i=1,2,\ldots,20$) locations at the adiabatic wall would have recorded if the triangular heat flux assigned by Eq. (4) was prescribed at the heated top channel wall. This dimensionless bottom wall temperature $\Theta_{Bd}(X_i)$, obtained from the solution of the direct problem with $\Delta X=0.005$ ($N=20$), is referred to as "exact" data and is used as an input to the inverse problem. With the velocity and temperature profiles being uncoupled for the forced convection problem considered, the velocity field U and V as determined from the above direct solution with $\Delta X=0.005$ ($N=20$) is stored for input to the inverse calculations at the 20 axial locations that the sensors are located.

Inverse Convection Problem

For the inverse convection problem, the temperature distribution of the insulated bottom wall $\Theta_{Bd}(X)$ is now provided as an input; whereas no information is available with regard to the heat flux or temperature variation of the top wall. Estimates for those quantities, namely $q_T(X)$ and $\Theta_T(X)$, constitute the objectives of the inverse methodology. Thus, the ther-

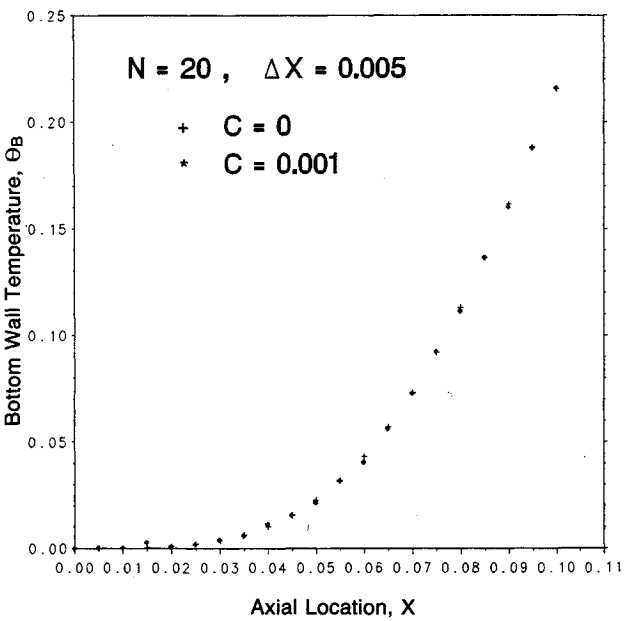

Fig. 2 "Exact" bottom wall temperature at the 20 sensor locations with and without superposed instrument errors.

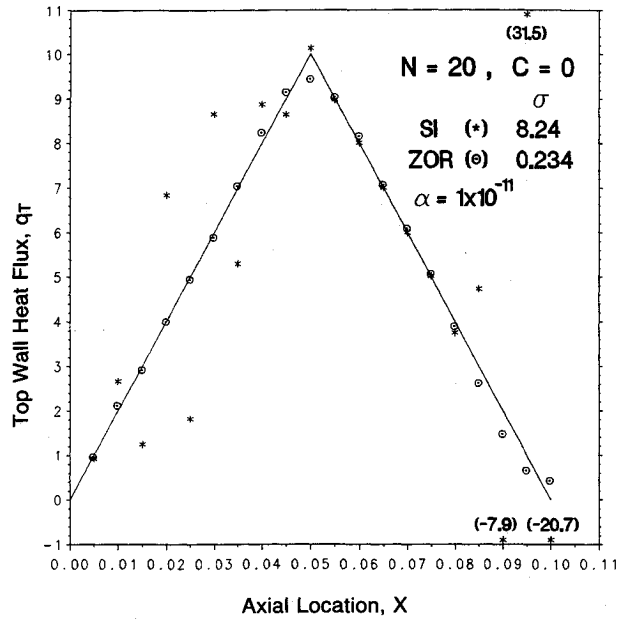

Fig. 3 Estimation of the top wall heat flux using 20 errorless sensors; —prescribed flux; straight inversion (SI); zeroth order regularization (ZOR).

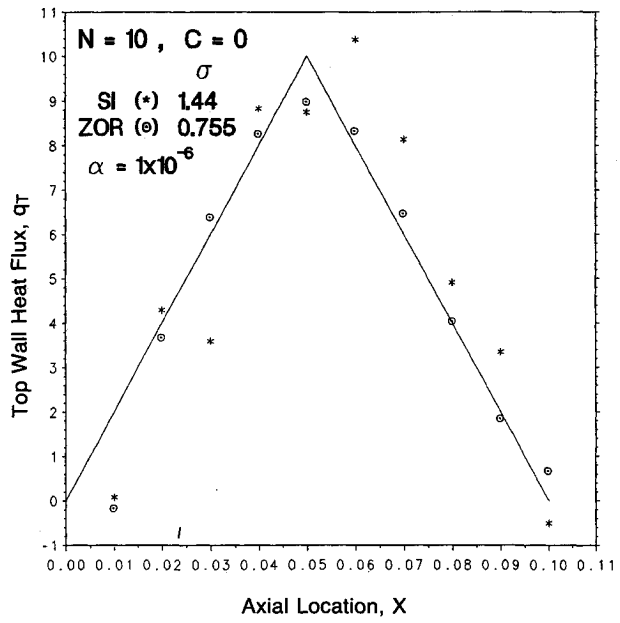

Fig. 4 Estimation of the top wall heat flux using 10 errorless sensors; —prescribed flux; straight inversion (SI); zeroth order regularization (ZOR).

mal boundary conditions appropriate for the direct problem, Eq. (3c), are now replaced by

$$\Theta = \Theta_B(X) \quad \text{at } Y = 1, \qquad \frac{\partial \Theta}{\partial Y} = 0 \quad \text{at } Y = 1 \qquad (3c')$$

where $\Theta_B(X)$ is the prescribed temperature variation of the bottom wall.

In the direct convection problem, a thermal boundary condition is prescribed for each surface; whereas the inverse problem involves the prescription of both boundary conditions on one surface. A standard procedure to circumvent this difficulty, referred to herein as the straight inversion, would utilize the solution algorithm of the direct problem along with a least squares method coupled with a Newton-Raphson iterative scheme.

When the exact bottom wall temperature data $\Theta_{Bd}(X_i)$ were prescribed in Eq. (3c′) for the inverse problem with all 20 sensors being active ($N = 20$, $\Delta X = 0.005$), the straight inversion scheme mentioned above produced the erratic oscillating heat flux for the top wall depicted with an asterisk (*) in Fig. 3. Thus, even when the input data for the bottom wall temperature are supplied from the direct solution without any superposed random errors, the straight inversion fails soundly in reproducing the triangular heat flux for the top wall prescribed by Eq. (4) and shown as a solid line in Fig. 3.

To assess the performance of the inverse methodology, a quantitative criterion can be established by defining a root mean square error of the dimensionless estimated top wall heat flux σ

$$\sigma = \left[\frac{1}{N}\sum_{i=1}^{N}(q_{T,i} - q_{Tc,i})^2\right]^{1/2} \qquad (5)$$

where q_T and q_{Tc} are, respectively, the prescribed (Eq. 4) and computed values of the dimensionless top wall heat flux. Thus, the straight inversion employing all 20 sensors produces an unacceptable root mean square error of $\sigma = 8.24$.

Now, starting from the first sensor, if every other sensor is made inactive, this would simulate a setup of attempting to predict the top wall heat flux using only 10 sensors spaced equally along the bottom wall with $\Delta X = 0.01$ and $N = 10$. The readings of these 10 errorless sensors would then correspond to the exact data $\Theta_{Bd}(X_i)$ at the 10 locations $X_i = X_2$, X_4, X_6, . . . , X_{20}, as depicted in Fig. 2 by the symbol + . The straight inversion using only 10 sensors with $\Delta X = 0.01$ provides the less erratic $\sigma = 1.44$ but still not quite satisfactory distribution denoted by an asterisk in Fig. 4.

If, furthermore, one uses only five equally spaced sensors located at $X_i = X_4$, X_8, X_{12}, X_{16}, and X_{20}, the straight inversion using the zero instrument error readings $\Theta_{Bd}(X_i)$ for the bottom wall temperature at these locations with $N = 5$ and $\Delta X = 0.02$, produced the mediocre distribution ($\sigma = 3.51$) shown by an asterisk in Fig. 5. It is worthwhile to note that in the inversion with $N = 10$ and $N = 5$ sensors, respectively, the exact velocity data U_i and V_i obtained with $\Delta X = 0.005$ ($N = 20$) and stored at the respective ten and five locations were utilized.

The poor performance of the straight inversion scheme with errorless data from the direct convection problem for all three cases deserves some attention. In all inverse heat transfer problems of which this author is aware, including inverse conduction problems[5] and the inverse convection problem,[1] the ill-posed nature of the straight inversion scheme was revealed by superposing random errors to the temperature data obtained from the direct solution. One would have expected the straight inversion employing the exact errorless input data Θ_{Bd} with $N = 20$ ($\Delta X = 0.005$) to predict the top wall heat flux with a negligible root mean square error instead of the unstable distribution (*) of Fig. 3. One would further expect that using fewer errorless sensors would deteriorate the performance of the straight inversion scheme with the distortion greatly depending on the degree of axial variation of the top wall heat flux.

The present results are indicative of the degree of severity of the ill-posedness of the inversion scheme to small random fluctuations apparently introduced via the numerical algorithm. It should be stated that the numerical calculations were carried out in double precision arithmetic. Thus, unless the exact triangular heat flux of the top wall as prescribed by Eq. (4) is assigned as the initial guess for the least squares method and Newton-Raphson iterative scheme, the solution converges to the erratic distribution (*) shown in Fig. 3. When fewer sensors are used, even though the lack of information at the now inactive sensors has a tendency to hinder the performance of the inversion process, the resulting larger axial stepsizes due to fewer sensors have a stabilizing effect on the inversion, and the root mean square error decreases as noted (*) in Fig. 4 for $N = 10$. The further decrease in the number of sensors to $N = 5$ results in a root mean square error which is larger than that for $N = 10$, as the lack of information of the inactive

sensors becomes more crucial than the subsequent stabilizing effect of larger axial stepsizes, as seen (*) in Fig. 5.

In an effort to verify the validity of the straight inversion algorithm used, the direct heat transfer problem was recomputed using an axial stepsize of $\Delta X = 0.01$ ($N = 10$). When the temperature of the bottom wall from the direct heat transfer solution with $\Delta X = 0.01$ ($N = 10$) was assigned to the inverse problem, the straight inversion algorithm with $N = 10$ reproduced the triangular top wall heat flux to a remarkably accurate degree with a root mean square error of better than $\sigma = 0.007$. Similarly, when the direct problem was solved using an axial stepsize of $\Delta X = 0.02$ ($N = 5$), the straight inversion with the errorless input data for the bottom wall temperature for $N = 5$ predicted the top wall heat flux extremely accurately with a root mean square error of less than $\sigma = 0.0002$. The above two tests, even though they do not convey any physically significant message, serve to verify the numerical credibility of the inversion algorithm and attribute the proneness to failure of the straight inversion scheme to the smallness of the axial stepsize utilized.

Whole Domain Regularization Technique

To correct the ill-posed nature of inverse problems, a regularization scheme devised by Tikhonov and Arsenin[3] is adapted for the convection problem considered. A detailed description of the procedure is given in Beck et al.,[5] and only a relevant summary is repeated here. The regularization procedure is a technique that modifies the least squares approach by adding factors to reduce the inherent oscillations of ill-posed problems. The whole domain regularization scheme which is best suited for elliptic differential equations involves the minimization of an augmented sum of squares function s

$$s = \sum_{i=1}^{N} (\Theta_{Bm,i} - \Theta_{Bc,i})^2 + \alpha \left[W_0 \sum_{i=1}^{N} q_{T,i}^2 + W_1 \sum_{i=1}^{N-1} (q_{T,i+1} - q_{T,i})^2 \right] \tag{6}$$

where again N is the number of grid points along the wall away from the inlet that coincide with the measurement stations, Θ_{Bm} and Θ_{Bc} are, respectively, the measured and computed temperatures of the bottom wall, and α is the regularization parameter. The summation in Eq. (6) that is preceded by W_0 is called the zeroth order regularization term. If $W_1 = 0$ the minimization of Eq. (6) is referred to as the zeroth order regularization procedure. In the same manner, the summation in Eq. (6) that is preceded by W_1 is called the first order regularization term, and if $W_0 = 0$, the procedure is referred to as the first order regularization method. Higher order terms involving second and higher differences of the heat flux components of the top surface q_T may be included in Eq. (6), but it is not as common. When the regularization parameter α is set equal to zero, exact matching is obtained, and the solution is sensitive to the ill-posed nature of inverse problems as it regresses to the straight inversion scheme. However, by properly selecting α, instabilities may be eliminated as the regularization terms tend to reduce the maximum magnitudes of estimated values of the top wall heat flux q_T.

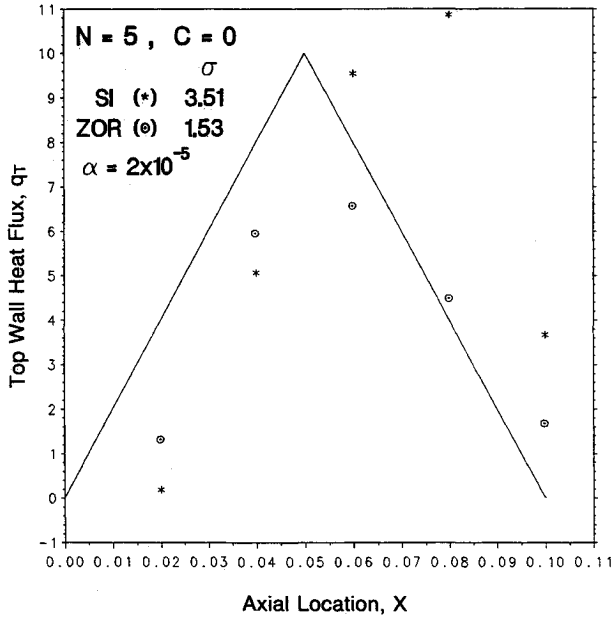

Fig. 5 Estimation of the top wall heat flux using five errorless sensors;—prescribed flux; straight inversion (SI); zeroth order regularization (ZOR).

To formulate the regularization procedure, the summation function s given by Eq. (6) is first minimized with respect to $q_{T,i}$, where $i = 1,2, \ldots j, \ldots N$, to give

$$\frac{\partial s}{\partial q_{T,1}} = 0 = -2(\Theta_{Bm,1} - \Theta_{Bc,1}) \frac{\partial \Theta_{Bc,1}}{\partial q_{T,1}} - 2(\Theta_{Bm,2} - \Theta_{Bc,2}) \frac{\partial \Theta_{Bc,2}}{\partial q_{T,1}} - \ldots\ldots - 2(\Theta_{Bm,N} - \Theta_{Bc,N}) \frac{\partial \Theta_{Bc,N}}{\partial q_{T,1}} + 2\alpha W_0 q_{T,1} + 2\alpha W_1 (q_{T,1} - q_{T,2}) \tag{7a}$$

$$\frac{\partial s}{\partial q_{T,j}} = 0 = -2(\Theta_{Bm,1} - \Theta_{Bc,1}) \frac{\partial \Theta_{Bc,1}}{\partial q_{T,j}} - 2(\Theta_{Bm,2} - \Theta_{Bc,2}) \frac{\partial \Theta_{Bc,2}}{\partial q_{T,j}} - \ldots\ldots - 2(\Theta_{Bm,N} - \Theta_{Bc,N}) \frac{\partial \Theta_{Bc,N}}{\partial q_{T,j}} + 2\alpha W_0 q_{T,j} + 2\alpha W_1 (-q_{T,j-1} + 2q_{T,j} - q_{T,j+1}) \quad \text{for } j = 2,3, \ldots, N-1 \tag{7b}$$

$$\frac{\partial s}{\partial q_{T,N}} = 0 = -2(\Theta_{Bm,1} - \Theta_{Bc,1}) \frac{\partial \Theta_{Bc,1}}{\partial q_{T,N}} - 2(\Theta_{Bm,2} - \Theta_{Bc,2}) \frac{\partial \Theta_{Bc,2}}{\partial q_{T,N}} - \ldots\ldots - 2(\Theta_{Bm,N} - \Theta_{Bc,N}) \frac{\partial \Theta_{Bc,N}}{\partial q_{T,N}} + 2\alpha W_0 q_{T,N} + 2\alpha W_1 (q_{T,N} - q_{T,N-1}) \tag{7c}$$

Next, since $\Theta_{Bc,i} = \Theta_{Bc,i}(q_{T,1}, q_{T,2}, \ldots, q_{T,N})$, one can expand from a Taylor series to get

$$\Theta_{Bc,i} = \Theta^*_{Bc,i} + \frac{\partial \Theta_{Bc,i}}{\partial q_{T,1}} \Delta q_{T,1} + \frac{\partial \Theta_{Bci}}{\partial q_{T,2}} \Delta q_{T,2} \ldots\ldots + \frac{\partial \Theta_{Bc,i}}{\partial q_{T,N}} + \Delta q_{T,N} \quad \text{for } i = 1,2, \ldots, N \tag{8}$$

where $\Theta^*_{Bc,i}$ denotes the current computed values of the bottom wall temperature based on the guessed values of the top wall heat flux $q^*_{T,i}$. The $\Delta q_{T,i}$ are the associated corrections to the guessed top wall heat flux and represent the main objective of the inversion algorithm since

$$q_{T,i} = q^*_{T,i} + \Delta q_{T,i} \qquad \text{for } i = 1,2, \ldots, N \tag{9}$$

Substituting for $\Theta_{Bc,i}$ and $q_{T,i}$, respectively, from Eqs. (8) and (9) into the system of Eqs. (7) and rearranging in a matrix form one gets

$$[A][Q] = [D] \tag{10}$$

In the above equation, the matrix of coefficients $[A]$ is given as the symmetric square matrix

$$
[A] = \begin{bmatrix}
\sum_{i=1}^{N} Z_{i,1}Z_{i,1} + \alpha(W_0 + W_1) & \sum_{i=1}^{N} Z_{i,1}Z_{i,2} - \alpha W_1 & \sum_{i=1}^{N} Z_{i,1}Z_{i,3} & \cdots & \sum_{i=1}^{N} Z_{i,1}Z_{i,j} & \cdots & \sum_{i=1}^{N} Z_{i,1}Z_{i,N} \\
\sum_{i=1}^{N} Z_{i,2}Z_{i,1} - \alpha W_1 & \sum_{i=1}^{N} Z_{i,2}Z_{i,2} + \alpha(W_0 + 2W_1) & \sum_{i=1}^{N} Z_{i,2}Z_{i,3} - \alpha W_1 & \cdots & \sum_{i=1}^{N} Z_{i,2}Z_{i,j} & \cdots & \sum_{i=1}^{N} Z_{i,2}Z_{i,N} \\
\sum_{i=1}^{N} Z_{i,3}Z_{i,1} & & & & & & \\
\vdots & & & & & & \\
\sum_{i=1}^{N} Z_{i,j}Z_{i,1} & & & \sum_{i=1}^{N} Z_{i,j}Z_{i,j-1} - \alpha W_1 & \sum_{i=1}^{N} Z_{i,j}Z_{i,j} + \alpha(W_0 + 2W_1) & \sum_{i=1}^{N} Z_{i,j}Z_{i,j+1} - \alpha W_1 & \sum_{i=1}^{N} Z_{i,j}Z_{i,N} \\
\vdots & & & & & & \\
\sum_{i=1}^{N} Z_{i,N-1}Z_{i,1} & & & & \sum_{i=1}^{N} Z_{i,N-1}Z_{i,N-2} - \alpha W_1 & \sum_{i=1}^{N} Z_{i,N-1}Z_{i,N-1} + \alpha(W_0 + 2W_1) & \sum_{i=1}^{N} Z_{i,N-1}Z_{i,N} - \alpha W_1 \\
\sum_{i=1}^{N} Z_{i,N}Z_{i,1} & & & & \sum_{i=1}^{N} Z_{i,N}Z_{i,N-1} - \alpha W_1 & & \sum_{i=1}^{N} Z_{i,N}Z_{i,N} + \alpha(W_0 + W_1)
\end{bmatrix}
$$

(11)

where $Z_{i,j}$ is the heat flux sensitivity coefficient of the bottom wall, defined by

$$Z_{i,j} \equiv \frac{\partial \Theta_{Bc,i}}{\partial q_{T,j}} \tag{12}$$

Also, in Eq. (10) the column matrix of unknowns for the top wall heat flux corrections $[Q]$ and the column matrix of constants $[D]$ are given, respectively, from

$$[Q] = \begin{bmatrix} \Delta q_{T,1} \\ \Delta q_{T,2} \\ \cdot \\ \cdot \\ \Delta q_{T,j} \\ \cdot \\ \cdot \\ \cdot \\ \Delta q_{T,N} \end{bmatrix} \tag{13}$$

$$[D] = \begin{bmatrix} \sum_{i=1}^{N} (\Theta_{Bm,i} - \Theta^*_{Bc,i}) Z_{i,1} - \alpha(W_0 + W_1) q^*_{T,1} + \alpha W_1 q^*_{T,2} \\ \sum_{i=1}^{N} (\Theta_{Bm,i} - \Theta^*_{Bc,i}) Z_{i,2} + \alpha W_1 q^*_{T,1} - \alpha(W_0 + 2W_1) q^*_{T,2} + \alpha W_1 q^*_{T,3} \\ \cdot \\ \cdot \\ \sum_{i=1}^{N} (\Theta_{Bm,i} - \Theta^*_{Bc,i}) Z_{i,j} + \alpha W_1 q^*_{T,j-1} - \alpha(W_0 + 2W_1) q^*_{T,j} + \alpha W_1 q^*_{T,j+1} \\ \cdot \\ \cdot \\ \cdot \\ \sum_{i=1}^{N} (\Theta_{Bm,i} - \Theta^*_{Bc,i}) Z_{i,N} + \alpha W_1 q^*_{T,N-1} - \alpha(W_0 + W_1) q^*_{T,N} \end{bmatrix} \tag{14}$$

In the computational procedure, guessed values are arbitrarily assigned for the dimensionless top wall heat fluxes

$$q_{T,i} = q^*_{T,i} \qquad \text{for } i = 1,2,\ldots,N \tag{15}$$

To estimate the sensitivity coefficients $Z_{i,j}$ defined from Eq. (12), the energy equation [Eq. (2d)] along with the associated thermal initial and boundary conditions, Eq. (15) for the top wall ($Y = 0$) and insulated condition for the bottom wall [Eq. (3c)] at $Y = 1$, are differentiated with respect to the dimensionless unknown heat flux of the top surface $q_{T,j}$. With $S_j \equiv \partial\Theta/\partial q_{T,j}$, there results for each $j = 1,2,\ldots, N$

$$U\frac{\partial S_j}{\partial X} + V\frac{\partial S_j}{\partial Y} = \frac{4}{PrRe^2}\frac{\partial^2 S_j}{\partial X^2} + \frac{1}{Pr}\frac{\partial^2 S_j}{\partial Y^2} \tag{16}$$

$$S_j = 0 \text{ at } X = 0, \quad \frac{\partial S_j^i}{\partial Y} = -\delta_{ij} \text{ at } Y = 0, \quad \frac{\partial S_j^i}{\partial Y} = 0 \text{ at } Y = 1$$

$$\text{for } i = 1,2,\ldots,N \tag{17}$$

In Eq. (17), δ_{ij} is the Kronecker delta. Equations (16) and (17) constitute a set of N systems of differential equations for the sensitivity function S_j for each $j = 1,2,\ldots, N$, where again N is the number of streamwise grid points along the wall away from the inlet. It is noted that due to the ellipticity of Eq. (16), the upstream nodal sensitivities do implicitly depend on the downstream sensitivity functions. Each set of Eqs. (16) and (17) was solved by the same Simpler algorithm[4] used for solving Eqs. (2) and (3). From the solution of each set ($j = 1,2,\ldots, N$) of Eqs. (16) and (17), and array of sensitivity coefficients $Z_{i,j}$ could then be determined, since from Eq. (12) and the definition of S_j one has

$$Z_{ij} = S_j^i \text{ at } Y = 1 \qquad \text{for } i = 1,2,\ldots,N \tag{18}$$

The solution algorithm for the inverse problem involves the following steps. First the velocity field U and V, as determined once from the solution of Eqs. (2a–2c) along with the boundary conditions Eqs. (3a) and (3b), is read as an input. Next, the top wall heat fluxes $q^*_{T,i}$ are arbitrarily guessed as in Eq. (15). The temperature field Θ is then solved from Eq. (2d) based on the guessed top wall heat fluxes and the adiabatic condition on the bottom wall, Eq. (3c). The sensitivity coefficients for the bottom wall $Z_{i,j}$ are estimated from Eq. (18) after solving for the sensitivity functions S_j from Eqs. (16) and (17). The top wall heat flux corrections $\Delta q_{T,j}$ can then be evaluated from Eq. (10). New estimates for the top wall heat fluxes are thus obtained from Eq. (9), and the procedure is repeated until the heat flux corrections become negligible, in this case smaller than 10^{-4}.

It is noted that even though the inverse problem considered in this study is linear, the procedure outlined in this section could be applied in exactly the same manner for nonlinear convection problems.

Results

To assess the success of the inversion scheme in curbing the ill-posed effects of the inverse convection problem manifested in Figs. 3, 4, and 5, the regularization algorithm was tested when the exact bottom wall temperature data $\Theta_{Bd}(X_i)$, obtained from the direct solution with $N = 20$ ($\Delta X = 0.005$), were prescribed in Eq. (3c′). When the regularization parameter α is set equal to zero, exact matching is obtained and the results are those of the straight inversion scheme depicted by an asterisk (*) in the three figures. Results for the top wall heat flux variation using a zeroth order regularization scheme, $W_0 = 1$, $W_1 = 0$ in Eq. (6) are depicted with the symbol ⊙ in the three figures. The regularization parameter was assigned the values of $\alpha = 1 \times 10^{-11}$, 1×10^{-6}, and 2×10^{-5}, respectively, in Figs. 3, 4, and 5, corresponding to the number of active sensors of $N = 20$, 10, and 5. In contrast to the highly oscillatory results of the straight inversion scheme (*) that tend to become unstable as the axial stepsizes decrease, relatively good agreement prevails in all three figures between the predictions of the regularization scheme (⊙) and the prescribed triangular top wall heat flux indicated by a solid line. The degree of success of the regularization scheme in curbing the ill-posed nature of the inversion process is manifested by the relatively low root mean square errors of $\sigma = 0.234$ for $N = 20$, $\sigma = 0.755$ for $N = 10$, and $\sigma = 1.53$ for $N = 5$ as shown in the

three figures. As expected the performance of the inversion scheme deteriorates as less information is provided with fewer sensors.

Of major significance to the success of the regularization scheme is the appropriate choice of the regularization parameter α and to a lesser extent the choice of the order of the regularization technique. For a given regularization order, the optimum value of α that results in the best match and minimum root mean square error for the top wall heat flux depends on the physical problem itself, the number of active sensors used (i.e., magnitude of axial stepsize), and the standard deviation of the random instrument errors, if any. The results of the regularization algorithm presented in Figs. 3, 4, and 5, correspond to the optimum estimates obtained with regard to both the order of regularization and the regularization parameter. To illustrate the effects of the regularization parameter and the regularization order on the effectiveness of the inversion algorithm, the root mean square error σ of the top wall heat flux predictions using, respectively, a zeroth order, a first order, and a combined zeroth plus first order regularization scheme ($W_0 = 1$, $W_1 = 1$), is plotted as a function of the regularization parameter in Fig. 6 for the setup with ten ($N = 10$) active errorless sensors.

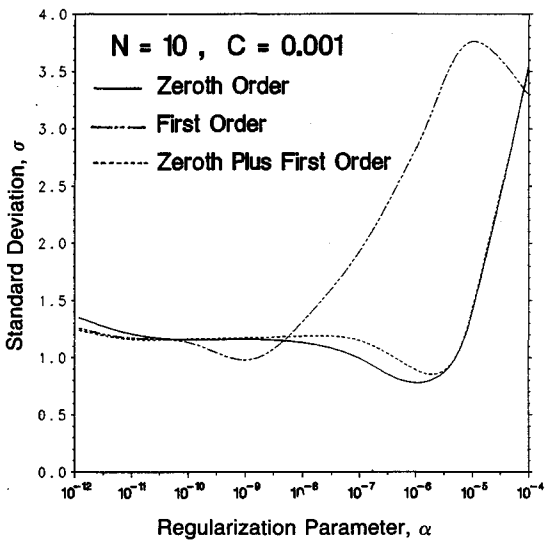

Fig. 6 Effect of the regularization parameter and the regularization order on the estimation of the top wall heat flux using 10 errorless sensors.

In practice, there are no perfect errorless sensors, and the bottom wall temperature variation is not prescribed from the solution of a direct problem but rather is acquired from local measurements that contain experimental errors. As such, the axial variation of the bottom wall temperature $\Theta_{Bm}(X)$, where subscript m denotes measured profile, will slightly differ than that of $\Theta_{Bd}(X)$. To account for this unavoidable discrepancy due to random errors inherent with any measuring device, the measured bottom wall temperature $\Theta_{Bm}(X)$ is simulated by superposing small random errors to the bottom wall temperature $\Theta_{Bd}(X)$ obtained from the solution of the direct problem.

$$\Theta_{Bm}(X_i) = \Theta_{Bd}(X_i) + \epsilon_i \tag{19}$$

The additive errors ϵ_i are written as

$$\epsilon_i = Ce_i \tag{20}$$

where e_i are the Gaussian random errors of mean zero and standard deviation of unity, and the constant C is chosen to make the standard deviation of ϵ_i equal to the desired value.

To illustrate the magnitude of the random noise, the bottom wall temperature data with superposed errors, $\Theta_{Bm}(X)$, are also depicted in Fig. 2 with the symbol * for a standard deviation of $C = 0.001$.

First, the straight inversion algorithm was implemented with random errors superposed on the bottom wall temperature obtained from the direct solution as implied from Eqs. (19) and (20). Results for the axial variation of the dimensionless heat flux of the top wall $q_T(X)$ for Gaussian random errors with standard deviation of $C = 0.001$ are shown in the insets of Figs. 7 and 8, and in Fig. 9, respectively, for each of the setups with $N = 20$, 10, and 5 active sensors. In each figure, the solid line represents the heat flux prescribed by Eq. (4). The top wall heat flux data predicted from the straight inversion, denoted by an asterisk (*) in each figure, possess the characteristics of ill-posed problems, i.e., highly oscillatory results that tend to become unstable as the axial stepsizes decrease. The root mean square errors for the top wall heat flux are of the order of $\sigma = 5 \times 10^5$ for $N = 20$, $\sigma = 262$ for $N = 10$, and $\sigma = 5.37$ for

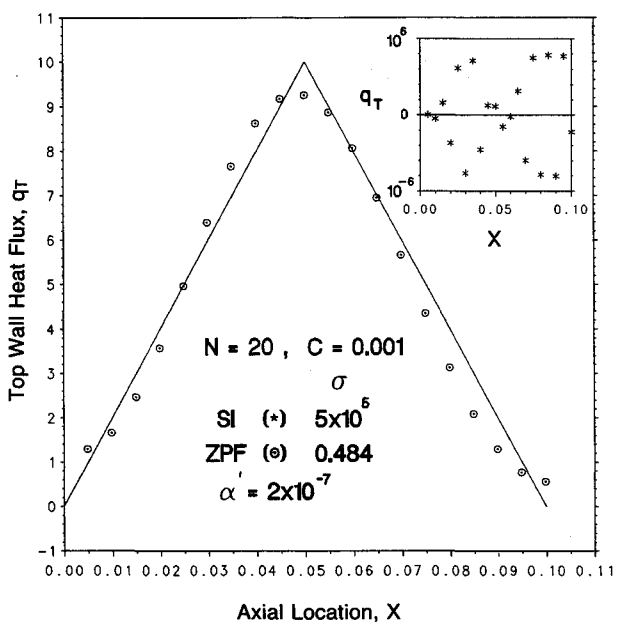

Fig. 7 Estimation of the top wall heat flux using 20 sensors with a standard deviation of $C = 0.001$;—prescribed flux; straight inversion (SI); zeroth plus first order regularization (ZPF).

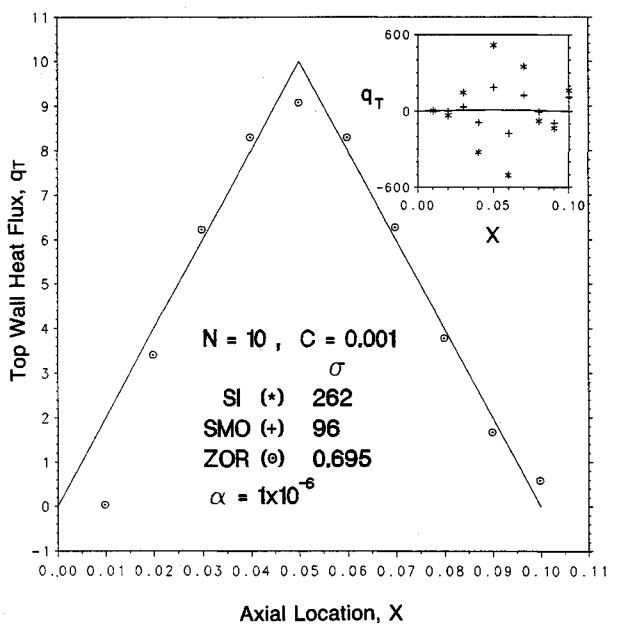

Fig. 8 Estimation of the top wall heat flux using 10 sensors with a standard deviation of $C = 0.001$;—prescribed flux; straight inversion (SI); smoothing (SMO); zeroth order regularization (ZOR).

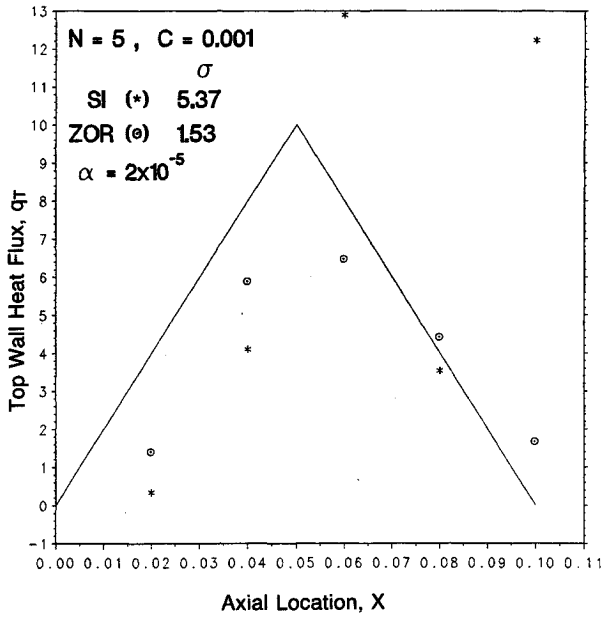

Fig. 9 Estimation of the top wall heat flux using five sensors with a standard deviation of $C = 0.001$;—prescribed flux; straight inversion (SI); zeroth order regularization (ZOR).

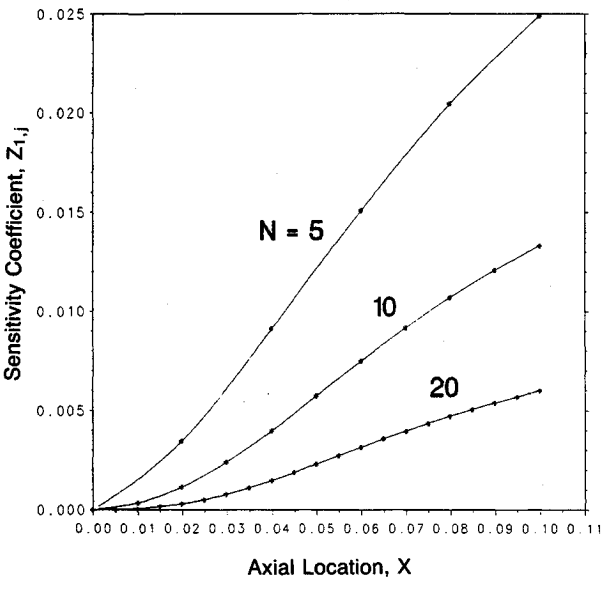

Fig. 10 Heat flux sensitivity coefficients of the bottom wall for the first sensor located at $X_1 = X_N/N$.

$N = 5$, significantly larger than the corresponding errors shown in Figs. 3, 4, and 5, when the straight inversion was utilized with zero instrument error sensors.

Next, the whole domain regularization technique was tested with random errors superposed on the bottom wall temperature in simulating sensor readings possessing instrument errors with a standard deviation again of $C = 0.001$. Optimum estimates for the top wall heat flux using the combined zeroth and first order regularization scheme ($W_0 = 1, W_1 = 1$) for the case of 20 active sensors ($N = 20$) are depicted in Fig. 7 with the symbol ⊙. The regularization technique is remarkably successful in curbing the magnification of the ill-posedness of the inversion due to instrument error of the sensors used for recording the bottom wall temperature. The root mean square error of the top wall heat flux is now a mere $\sigma = 0.484$.

Optimum results for the top wall heat flux employing, respectively, only 10 active sensors ($N = 10$) and five active sensors ($N = 5$) with standard deviation of $C = 0.001$ were obtained using the zeroth order regularization scheme ($W_0 = 1$, $W_1 = 0$). These estimates are depicted, respectively, in Figs. 8 and 9 with the symbol ⊙ providing corresponding root mean square errors of $\sigma = 0.695$ for $N = 10$ and $\sigma = 1.53$ for $N = 5$. As observed before, the performance of the regularization procedure deteriorates as fewer active sensors are utilized in the inversion process. A comparison among the root mean square errors employing the same number of sensors with and without measurement errors reveals that the effectiveness of the regularization procedure becomes insensitive to instrument errors as fewer sensors (larger stepsizes) are utilized.

The sensitivity of the inversion scheme to the sensor interspace and number of sensors employed can be established from a study of the sensitivity coefficients $Z_{i,j}$. Such a study provides valuable information in the design of the experimental setup as the total number of streamwise grid points N and related axial stepsizes utilized in the inversion scheme correspond directly to the number of sensors and sensor interspace employed. As the velocity and temperature profiles are uncoupled for the forced convection problem considered, the sensitivity coefficients obtained via the solution of Eqs. (16) and (17) are independent of the temperature solution and consequently of the standard deviation C of the random measurement errors of the bottom wall temperature.

The streamwise variation of the bottom wall sensitivity coefficient for the first sensor $Z_{1,j}$, located at $X_1 = X_N/N$, is illustrated in Fig. 10 for each of the three various setups with corresponding number of sensors of $N = 20$, 10, and 5, respectively. With the sensitivity coefficient $Z_{i,j}$ being a measure of the information available with regard to the heat flux at X_i from all the sensors located at $X_j, j = 1,2,\ldots N$, the degree of the severity of the ill-posedness of the inversion process is inversely proportional to the magnitude of the sensitivity coefficients. The smaller the sensor interspaces (larger N) the smaller the corresponding sensitivity coefficients and the larger susceptibility to measurement errors. This is manifested via the magnitude of the root mean square errors σ of the predicted top wall heat fluxes illustrated in Figs. 7, 8, and 9, when the straight inversion is used with random instrument errors of standard deviation $C = 0.001$. Thus, the setup with only five active sensors ($N = 5$) results in the largest sensitivity coefficients and the smallest, but yet unsatisfactory, root mean square error of $\sigma = 5.37$ (Fig. 9). As the number of active sensors increases to the respective setups of $N = 10$ and 20, the smaller sensitivity coefficients signify larger susceptibility of the inversion scheme to measurement errors as attested from the rapidly increasing order of magnitude of the root mean square errors shown in Figs. 8 and 7, respectively. Of course, the obvious disadvantage of large stepsizes (small N) is their inability to yield pertinent information with regard to abruptly changing top wall heat flux variations as witnessed from Fig. 9.

The axial variation of the bottom wall sensitivity coefficients for all the sensors for the case of $N = 10$ are plotted in Fig. 11. The sensitivity coefficients decrease with downstream located sensors as the curves are displaced ΔX apart. As seen from the figure, since $Z_{i,j}$ is approximately equal to zero for $j < i$, little or no information is available with regard to the heat flux at X_i from the upstream sensors. This is also an indication that the ellipticity of the sensitivity equation via the axial diffusion term, Eq. (16), is not severe.

Finally, the accuracy of a simple smoothing procedure is tested by comparison with the results of the regularization scheme. The procedure involves the initial smoothing of the data for the bottom wall temperature profile containing random instrument errors coupled with a straight inversion scheme. After having added the random errors to the bottom wall temperature obtained from the direct solution, the noisy data were smoothed using a cubic spline data smoother (IMSL subroutine ICSSCV) that required no special information with regard to the input data. The ICSSCV routine calculates a

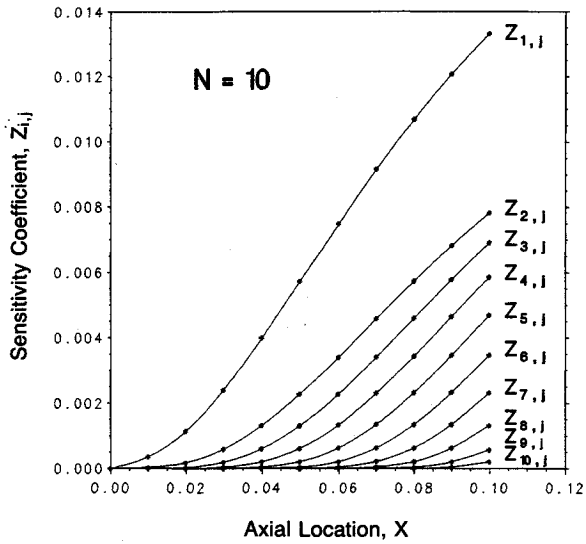

Fig. 11 Heat flux sensitivity coefficients of the bottom wall for all 10 sensors used.

cubic spline curve which smooths a given set of data points employing statistical considerations in determining the amount of smoothing required.[6] The predictions of the direct straight inversion algorithm for the top wall heat flux using the smoothed data as an input for errors with standard deviation of $C = 0.001$ and for the case of $N = 10$ are depicted with the symbol + in the inset of Fig. 8. As can be attested from the figure and the magnitude of the associated root mean square error, $\sigma = 96$, the initial smoothing of the corrupted data and the subsequent straight inversion produce a smaller root mean square error than the case with no smoothing but fail to alleviate the unsteady oscillations inherent with direct inversion schemes of ill-posed problems. This is in contrast to the commendable performance of the same smoothing routine in the related inverse free convection problem.[1] The inconsistency in the performance of the smoothing routine is due to its dependence on the severity of the ill-posedness of the inverse problem. Neither the whole domain regularization scheme used in this study nor the sequential function specification scheme employed in Ref. 1 suffer from such a condition. When a large number of sensors are implemented, the performance of the whole domain regularization scheme may be improved if the error containing data are initially treated with a smoothing routine like the one employed in this study.

Summary

It is important to note that the aforementioned trends and discussion with regard to the performances of the straight inversion and whole domain regularization schemes are pertinent to the specific problem and prescribed conditions imposed. For the parameters considered, the present study illustrates that the inverse problems may be extremely sensitive to inherent fluctuations introduced during the numerical computations and/or inherent random experimental errors.

The whole domain regularization scheme that is tailored for elliptic inverse problems is shown to successfully curb the ill-posed symptoms of the weakly elliptical inverse convection problem considered. The choice of the regularization parameter is found to significantly affect the performance of the inversion algorithm, and the determination of the optimum value of α in a real situation may require some knowledge on the basic shape of the unknown heat flux and/or an estimate of the measurement errors. Sensitivity coefficients that are indicative of the severity of the ill-posedness of the inverse problem are illustrated for the three setups considered. Finally, a simple initial smoothing of the tampered input data for the bottom wall temperature along with a straight inversion scheme fail to rid the ill-posed symptoms associated with inverse problems.

References

[1]Moutsoglou, A., "An Inverse Convection Problem," *Journal of Heat Transfer,* Vol. 111, No. 1, 1989, pp. 37–43.

[2]Beck, J. V., "Nonlinear Estimation Applied to the Nonlinear Heat Conduction Problem," *International Journal of Heat and Mass Transfer,* Vol. 13, No. 4, 1970, pp. 703–716.

[3]Tikhonov, A. N. and Arsenin, V. Y., *Solutions of Ill-Posed Problems,* Winston, Washington, DC, 1977.

[4]Patankar, S. V., *Numerical Heat Transfer and Fluid Flow,* Hemisphere, Washington, DC, 1980.

[5]Beck, J. V., Blackwell, B., and St. Clair Jr., C. R., *Inverse Heat Conduction, Ill-Posed Problems,* Wiley-Interscience, New York, 1985.

[6]Craven, P. and Wahba, G., "Smoothing Noisy Data with Spline Functions," *Numerische Mathematik,* Vol. 31, 1979, pp. 377–403.